Separation and Purification Technology 339 (2024) 126685

Contents lists available at ScienceDirect

Separation and Purification Technology

journal homepage: www.elsevier.com/locate/seppur

Photoinduced enhanced CO_2 capture performance on carbon-doped boron nitride adsorbent

Xiaoyu Duan [a,b], Guanqing Song [b], Chi Song [b], Guanhong Lu [b], Yan Wang [b], Jing Sun [b], Aiying Chen [a,*], Xiaofeng Xie [b,*]

[a] University of Shanghai for Science and Technology, 516 Jungong Road, Shanghai 200093, China
[b] Shanghai Institute of Ceramics, Chinese Academy of Sciences, 585 Heshuo Road, Shanghai 201800, China

ARTICLE INFO

Keywords:
CO_2 capture
Boron nitride
Photoinduced
Adsorption
Regeneration

ABSTRACT

The key issues in the CO_2 capture industry are the high energy and cost consumption during the capture and regeneration process. Enhancing CO_2 adsorption and rapid desorption through switches sunlight irradiation is a promising route. In this study, a series of carbon-doped boron nitride (BCN) adsorbents with different contents were synthesized. The BCN presented a growing CO_2 adsorption capacity under light irradiation, implying that sunlight may become a key driving force for the low-cost CO_2 capture. During the experiments, the best performing sample BCN(1:3) showed 32 % and 28 % increase in CO_2 adsorption capacity after UV light irradiation at 0.15 and 1 bar CO_2 pressure, respectively. To explain this interesting phenomenon, a series of tests and analyses had been conducted, such as EPR, Hall effect test and DFT computation. The results confirmed that the enhanced CO_2 absorption characteristics can be attributed to the photoelectric effects of generating more free electrons, which enhanced Lewis alkalinity of BCN adsorbents and thus improved their CO_2 adsorption capacities. This work, for the first time, utilizes the photoelectric effect to increase the efficient capture capacity of CO_2, opening up a new path for the design and research of CO_2 capture materials.

1. Introduction

In recent years, climate change caused by the greenhouse effect has become a major global challenge, and the frequency of extreme weather events is also increasing. Most researchers believe that CO_2 is the main factor causing the greenhouse effect, so carbon neutrality strategies have attracted increasing research interest.[1,2] High-efficient and low-cost methods for separating, capturing, storing, and converting CO_2 are being widely studied. The usual CO_2 capture method is wet washing with strong alkaline liquid.[3] However, some issues with this method, such as equipment corrosion, operational risks, and significant regeneration costs, limit its industrial applications.[4] Therefore, developing fast, efficient, and environmentally friendly CO_2 solid adsorption materials and low-cost regeneration methods has also become very important.

Boron nitride (BN) nanomaterials are excellent functional materials for optoelectronics with excellent physical properties, high thermal conductivity and high oxidation resistance.[5,6] These properties make them very promising for various potential applications in areas such as optoelectronic nanodevices, photocatalysts and functional composites.[7–10] In addition, BN nanomaterials have great potential for application in the field of CO_2 capture. The poor CO_2 adsorption capacity of pristine BN nanomaterials is mainly due to the weak interaction between electron-deficient BN and Lewis acidic CO_2. However, element doping, surface modification, or composite modification can effectively improve the CO_2 capture performance of BN materials.[11–13] In order to improve the CO_2 adsorption capacity of BN adsorbents, it is crucial to change their electronic structure.[14] It has been reported that carbon can be doped into BN adsorbents to produce $B_xC_yN_z$ materials, which is thought to modulate the electronic structure of BN materials, thus giving more active defects in BN materials.[15–17] This $B_xC_yN_z$ material is considered to possess some characteristics of both hexagonal boron nitride (h-BN) and graphene, such as containing both graphene and h-BN structural domains, and its band gap can be modulated by changing its doping concentration.[18,19].

Meanwhile, CO_2 as a Lewis acidic molecule, it prefers to accept electrons rather than give them during the reaction. We can control the adsorption/desorption of CO_2 in BN nanomaterials by changing the

---

* Corresponding authors.
E-mail addresses: aychen@usst.edu.cn (A. Chen), xxfshcn@163.com (X. Xie).

https://doi.org/10.1016/j.seppur.2024.126685
Received 25 December 2023; Received in revised form 2 February 2024; Accepted 2 February 2024
Available online 5 February 2024

charge state of BN nanomaterials. Light energy is a renewable and clean energy source that combines the photoelectric properties of BCN with adsorption properties. It is an attractive work to change the electronic structure of BCN by light for photo-controlled CO_2 adsorption/desorption.

Here, we achieved in situ carbon doping of BN materials by synthesizing BCN under N_2 atmosphere using a simple pyrolysis method. And found that the band gap structure of BCN materials can be controlled by changing the ratio of the medium raw materials. Based on the unique photovoltaic properties of BCN materials, we had enhanced the adsorption capacity of BCN adsorbents by irradiating them with UV lamps under different CO_2 partial pressure conditions for the first time. And various characterization analyses of this novel phenomenon were carried out to explain the feasibility of photo-irradiated BCN materials for enhancing CO_2 adsorption.

2. Materials and methods

2.1. Materials and chemicals

Melamine ($C_3H_6N_6$, 99 %) and barium sulfate ($BaSO_4$, 99.99 %) were purchased from adamas-beta (Shanghai, China) Chemical Reagent Co. Boric acid (H_3BO_3, 99.5 %) was purchased from Shanghai Tongya Chemical Technology Development Co. Hexagonal boron nitride (h-BN, 99.5 %,325 mesh powder) was purchased from Alfa Aesar (China) Chemical Co. SBA-15 molecular sieve (99 %) was purchased from Jiangsu Xianfeng Nanomaterials Technology Co. The gases used in this study, Ar (99.999 %), N_2 (99.99 %) and CO_2 (99.99 %) were purchased from Shanghai Guanglin Gas Co. Deionized water was used in the synthesis and testing process.

2.2. Synthesis of BCN adsorbents

A series of BCN adsorbents with different raw material ratios were synthesized using boric acid (H_3BO_3) and melamine ($C_3N_6H_6$) as the boron and nitrogen sources, respectively. Specifically, 1.5 g of H_3BO_3 was dissolved in 150 ml of deionized water at 60 ℃ with constant stirring until the solution was clarified. Then a certain amount (4.5 g, 3 g, 1.5 g, 0.5 g) of $C_3N_6H_6$ was added to the above solution, and the obtained solution was heated to 90 ℃ with continuous stirring until a transparent solution was formed. The obtained transparent solution was then heated in an electric blast furnace at 90 ℃ for 15 h, and then the obtained white solid was ground into powder. Finally, the collected white powder was loaded into a tube furnace and heated to 800 ℃ in an N_2 atmosphere with a heating rate of 2 $℃\cdot min^{-1}$ for 6 h. The obtained powder adsorbent was denoted as BCN(x:y) (x:y is the mass ratio of boric acid to melamine). The preparation process of BCN material is shown in Figure S1.

2.3. Characterization methods

The synthesized porous BCN adsorbents were characterized by various methods.

The adsorbents were X-ray diffracted (Ultima IV, Ritani, Japan) using Cu $K_{\alpha1}$ radiation ($\lambda = 0.15418$ nm) with a scanning speed of 8°/min and a range of 10-90°for 2θ.

The BCN adsorbent was tested with a UV/Vis/NIR spectrophotometer (lambda 1050+, Perkin-Elmer, USA) in the absorption mode of 200–800 nm to determine the UV–visible band light absorption of the BCN material. Prior to each test, a background scan was performed using a $BaSO_4$ press sheet, and then the BCN adsorbents press sheet was analyzed.

FT-IR (Fourier transform infrared) spectroscopy was performed with an infrared spectrometer (Spotlight 400, Perkin-Elmer, USA) in the absorption mode of 4000 ~ 400 cm^{-1} to determine the chemical bonds and groups of the BCN material. The adsorbents were mixed with potassium bromide and then pressed into flakes for analysis.

Raman spectra of BCN absorbers were obtained using a Raman spectrometer (in Via, Renishaw, UK) with a He-Ne laser at 780 nm with an excitation power of 0.5 mW and a 1200 l/mm grating.

The X-ray photoelectron spectra (XPS) of the adsorbents were monitored by an X-ray photoelectron spectrometer (ESCAlab250, Thermo Fisher Scientific, USA), and the adsorbents were all surface etched by Ar ion beam before testing. Charge correction was performed with a C 1s photoelectron peak at 284.6 eV. The XPS peaks were deconvoluted using XPS Peak software.

The morphology and structure of the adsorbents were photographed by high resolution transmission electron microscopy (HRTEM) (JEM-2100F, Jeol, Japan) and field emission scanning electron microscope (FESEM) (S-4800, Hitachi, Japan) and energy dispersive X-ray energy spectroscopy (EDS). The adsorbents were dispersed in ethanol by ultrasound, deposited on perforated ultrathin carbon films, and then subjected to HRTEM analysis.

The nitrogen adsorption–desorption isotherms of the BCN-based adsorbents were measured with a volumetric gas adsorption analyzer (Autosorb iQ, Quantachrome, USA) to determine the mesoporous (2–50 nm) and macroporous structures (>50 nm). Prior to analysis, the adsorbents were degassed at 120 ℃ under vacuum for 6 h.

The Hall coefficient and carrier concentration changes of BCN(1:3) adsorbent before and after 365 nm UV irradiation were measured with a Hall effect tester (HMS-7000, ECOPIA, Korea). After the light-free condition test, the adsorbents were irradiated under UV lamp for 2 h, and the Hall effect was tested again after the lamp was turned off for about 2 min.

CO_2-TPD (Temperature Programmed Desorption) was measured in a chemisorption analyzer (PCA-1200, Builder, China) with a quartz tube reactor and thermal conductivity (TCD) to determine the basic center of the BCN(1:3) adsorbent. Specifically, 50 mg of adsorbent was degassed in N_2 (30 $ml\cdot min^{-1}$) at 200 ℃ for 1 h. After cooling to room temperature (25 ℃), high-purity CO_2 (40 $ml\cdot min^{-1}$) was introduced and adsorbed for 2 h to reach adsorption equilibrium. Then the adsorbent was heated to 800 ℃ in N_2 (30 $ml\cdot min^{-1}$) at a heating rate of 10 $℃\cdot min^{-1}$ and kept for 10 min, and the desorbed CO_2 was detected by a thermal conductivity detector (TCD).

The adsorbents were analyzed by in situ light analysis using a paramagnetic resonance spectrometer (EMXnano, Bruker, Germany) with a mercury lamp source (LOT-QuantumDesign GmbH) in the wavelength range of 200–2000 nm.

Electrochemical tests were carried out on a CHI-660D electrochemical workstation with ITO glass, platinum wire, Ag/AgCl as working electrode, counter electrode and reference electrode, respectively. Before preparing the working electrode, 10 mg of powder adsorbent was dispersed into 1 ml of ethanol, 50 μL of Nafion solution with a mass fraction of 5 % was added and sonicated for 30 min to form a homogeneous suspension. Then, the suspension was coated on ITO glass and dried at room temperature. In addition, the electrolyte was 0.5 M Na_2SO_4 aqueous solution and the light source was a 365 nm UV lamp (Power 30 W).

2.4. CO_2 adsorption measurements

CO_2 adsorption was performed on an iSorb HP2 instrument (Quantachrome Instruments) at 298 K. High purity grade carbon dioxide (99.99 %) was used for all adsorption measurements. Prior to the measurements, the adsorbents were pretreated at 120 °C under vacuum for 6 h. And the light source was a 365 nm UV lamp (Power 30 W). The temperature increase of the material after irradiation with 365 nm UV light is not more than 2 ℃.

2.5. Theoretical calculation

The DFT calculations were performed using the VASP software

(Specific calculations are in the SI theoretical calculations section). And the elemental ratios of the model were matched to those of the actual BCN (1:3) adsorbent, where the atomic numbers B:C:N:O = 16:10:15:19. The injection of extra electrons in the DFT is added directly through the NELECT setting in the VASP software. It is worth mentioning that the DFT calculations in this work were confined to the introduction of 1 extra electron in a very small localized region. Therefore, the impact on the system is significant. In practical experiments more free electrons are produced after light irradiation, however the vast majority of the electrons will quickly complex with holes and disappear. And only a small fraction of the surface photo-generated free electrons will persist and play a role in the light-induced adsorption enhancement.

3. Results and discussion

3.1. Characterization of BCN adsorbents

The morphology of the BCN adsorbents was investigated using SEM and TEM. SEM images show that the main bodies of the synthesized BCN adsorbents all display micron-scale band morphology (Fig. 1a and Figure S2), which is typical of BCN morphology obtained from precursor pyrolysis at high temperatures.

TEM images show that the BCN(1:3) adsorbents consist of a number of band stacks as well as multilayer graphene-like sheets. Also, a uniform distribution of porous structures on the surface can be observed, this phenomenon also observed in other BCN adsorbents (Fig. 1b and Figure S3). These porous structures are mainly caused by the release of ammonia, carbon monoxide, nitrogen and some cyanide gas bubbles during the pyrolysis of the adsorbents.[1,20] With increasing melamine, the crystallinity of BCN(1:1), BCN(1:2) and BCN(1:3) gradually decreased and the vortex layer structure became more pronounced (Figure S4). The microscopic morphology of the worm-like microporous network can be seen by HRTEM images, while the local FFT (Fast Fourier Transform) transformation was performed to obtain an amorphous-like diffraction pattern (Fig. 1c).

The BCN(1:3) adsorbent whose corresponding EDS elemental mapping image is shown in Fig. 1d. The elements B, C, N and O are uniformly distributed in the selected region, indicating that the BCN(1:3) adsorbent has residual carbon and abundant oxygen-containing functional groups.

XRD images of BCN adsorbents with different raw material ratios were shown in Fig. 2a. The adsorbents show two broad diffraction peaks near 2θ around 26° and 43°, which are attributed to the (0 0 2) and (1 0 0) facets (PDF#34–0421) of h-BN, respectively.[21,22] The peak near 26° is graphite-like layer stacking, and the peak at 42.5° is associated with in-plane repeating units. All peaks are broad and narrow, indicating defect-rich or turbo structures.[22] As the ratio of boric acid/melamine in the raw material decreases, the intensity of the corresponding diffraction peaks on the adsorbent (0 0 2) surface decreases gradually; the peak widths become broader and move to lower 2θ values. This indicates that as the melamine ratio in the raw material increases, it leads to the introduction of more carbon, producing more structural defects and increased interlayer distance.[1,23] The results indicate that the preparation of BCN by pyrolysis is successful.

Fig. 2b shows the FTIR spectra of a series of BCN adsorbents. The spectrum at ∼ 1398 cm^{-1} is attributed to in-plane B-N stretching vibrations from h-BN, and it can be found that their signal decreases correspondingly with the decrease of the boric acid/melamine ratio. This is due to the fact that the C atoms in melamine replace the B atoms in boron nitride, thus causing the strength of the B-N bond to decrease with increasing melamine content. The peak located at ∼ 768 cm^{-1} can be attributed to the out-of-plane B-N-B bending vibration,[24] and the peak here is only observed in the adsorbent of BCN (3:1). This was attributed to the fact that BCN (3:1) had the least amount of carbon doping and the lowest degree of disorder, and thus could still maintain a certain h-BN structure. The result is consistent with the previous XRD results that the adsorbent gradually transforms from h-BN (wide band gap) to graphene (zero band gap) as the melamine content in the raw material increases. And BCN materials belongs to the intermediate of both materials, the ideal medium bandgap BCN material can be

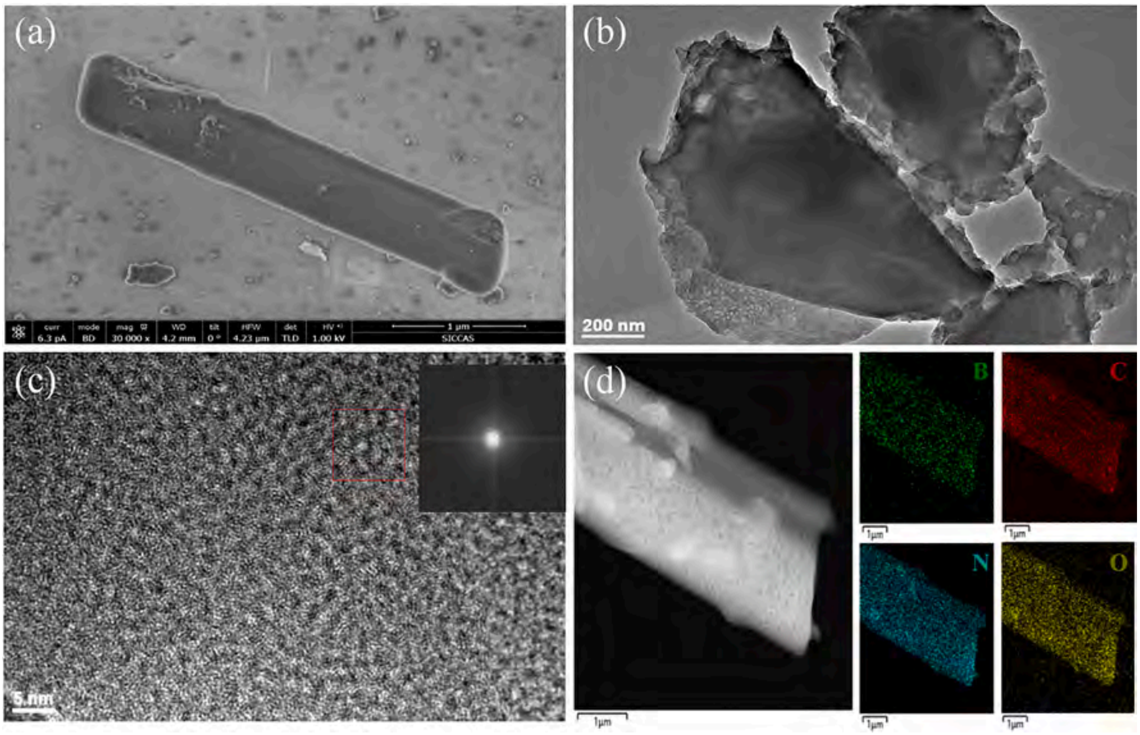

Fig. 1. (a) SEM image of BCN(1:3); (b) TEM image of BCN(1:3); (c) HRTEM image of BCN(1:3), the amorphous diffraction pattern in the upper right corner is obtained by local (red box) FFT transformation; (d) EDS diagrams of B,C,N and O elements of BCN(1:3). (For interpretation of the references to color in this figure legend, the reader is referred to the web version of this article.)

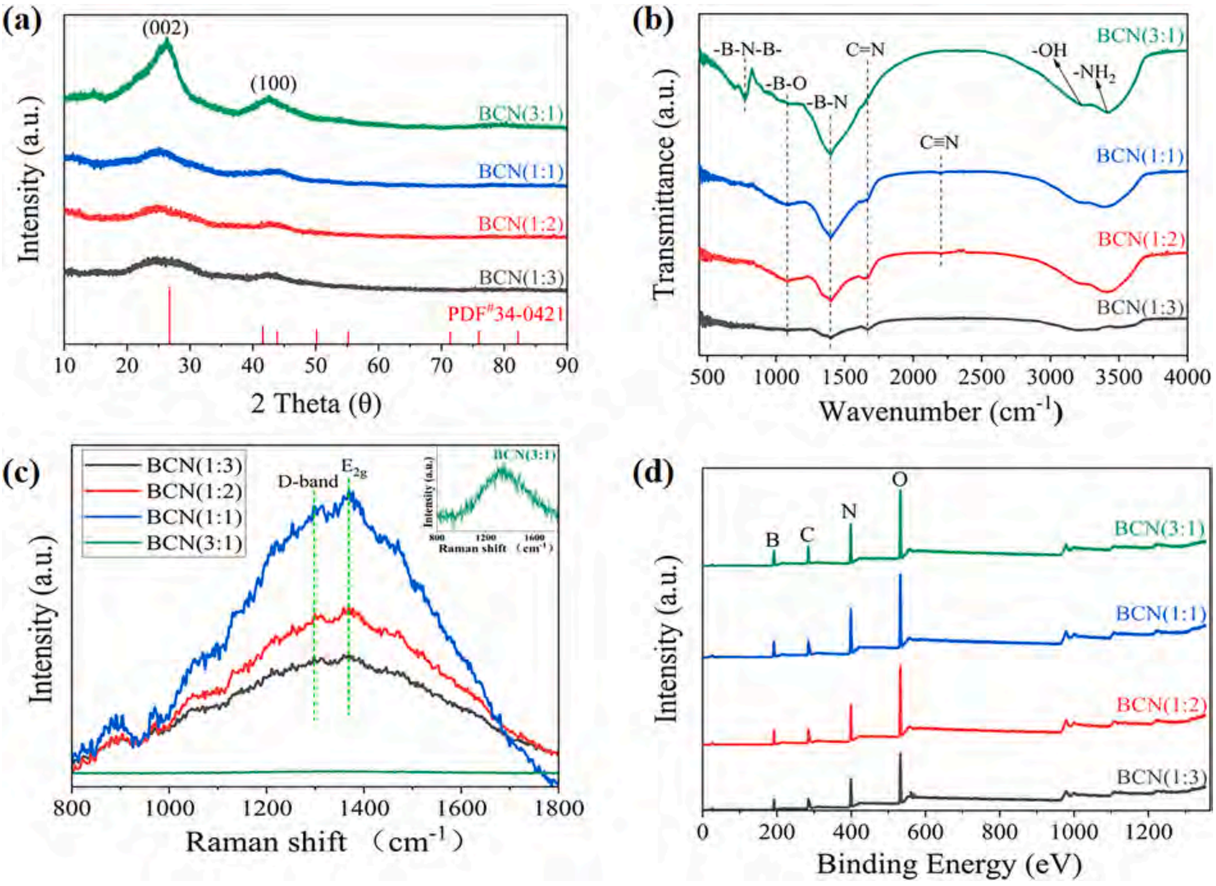

Fig. 2. (a) XRD pattern of BCN adsorbent; (b) FTIR spectrum of BCN adsorbent; (c) Raman pattern of BCN adsorbent; (d) XPS spectrum of BCN adsorbents.

synthesized by adjusting the raw material ratio. In addition, the peak at ~ 1080 cm^{-1} can be attributed to the absorption band of -B-O.[25] The position of the C = N absorption peak was detected near ~ 1670 cm^{-1}.[24] And a very faint small peak can be observed at ~ 2207 cm^{-1} attributed to the stretching vibration of C≡N,[26] this small peak is only observed in BCN (1:1) and (1:2). From BCN (3:1) to BCN (1:2), there is a constant increase in melamine in the feedstock and therefore a gradual increase in the carbon content of the product. The C atoms continue to displace the B atoms in the boron nitride and bond with N in a variety of bonding modes including C = N as well as C≡N. While in BCN (1:3) sample, the high content of C atoms may make the C≡N bonding content in the surface layer of the sample almost disappear, making it difficult to detect the corresponding C≡N bonding signals by IR instruments. The broad absorption bands at ~ 3209 cm^{-1} and ~ 3430 cm^{-1} should be attributed to –OH and –NH_2, respectively.[27].

The Raman spectrum of BCN adsorbent is shown in Fig. 2c. The synthesized BCN adsorbents all have a distinct peak near 1367 cm^{-1}, which is a typical Raman E_{2g} peak for h-BN. Meanwhile the peak near 1296 cm^{-1} can be attributed to the D peak of the carbon atom, which mainly originates from the stretching vibration of the C–C bond and the C = C double bond. And the intensity of the D peak reflects the proportion of defects, structural distortions, and amorphous portions in the sample.[28] Therefore, this can prove that there are more disordered carbon structures present in the material, with a consequent increase in the degree of defects. However, the diffraction intensity of BCN(3:1) was very different from the other three BCN adsorbents.[21] This is due to the fact that BCN(3:1) has the lowest carbon content compared to the other three adsorbents (Table 1) and the highest crystallinity, so the signal of the peak reflecting the degree of disorder in the crystalline structure of the material in it is very weak. In BCN(1:1), BCN(1:2) and BCN(1:3), the intensity of the Raman peak signal, which represents the vibration mode of the B-N bond between the h-BN layers, gradually decreases because their carbon content gradually increases and the degree of structural disorder also increases, and this result is consistent with the FTIR results.

Table 1
Relative contents of B, C, N and O species of BCN absorbents obtained by XPS surface analysis.

Adsorbents	Boron (wt. %)	Carbon (wt. %)	Nitrogen (wt. %)	Oxygen (wt. %)
BCN (1:3)	27.44	17.33	24.87	30.36
BCN (1:2)	29.13	15.20	23.87	31.80
BCN (1:1)	30.83	14.14	26.30	28.74
BCN (3:1)	35.92	12.50	22.50	29.08

The surface chemical states of the BCN adsorbents were analyzed by XPS technique. Signals of B 1s, C 1s, N 1s and O 1s were clearly found in the XPS measured spectra of BCN(3:1), BCN(1:1), BCN(1:2) and BCN (1:3) (Fig. 2d). The four elements of the relative contents are listed in Table 1. Fig. 3(a)-(d) show the deconvolution of the XPS spectra of each chemical element. As shown in Fig. 3(a), the high-resolution B 1s spectra can be deconvoluted into three peaks corresponding to B species in different chemical environments. Two signal peaks at 190.3 eV and 191.0 eV can be attributed to the characteristics of the B-N3 and O-B-N2 structures.[22] The binding energy peak at 192.1 eV belongs to the bonding feature of the B-O bond.[29–31] The structural features belonging to the B-C bond at 189 eV are only observed in the BCN (3:1) adsorbent, while the presence of C-B bond at 283 eV is only observed in the C 1s spectrum for the BCN (3:1) adsorbent.[23] The C 1s spectra of BCN adsorbents with different raw material ratios (Fig. 3b) can be mainly deconvoluted into four peaks in the bonding configurations of C-

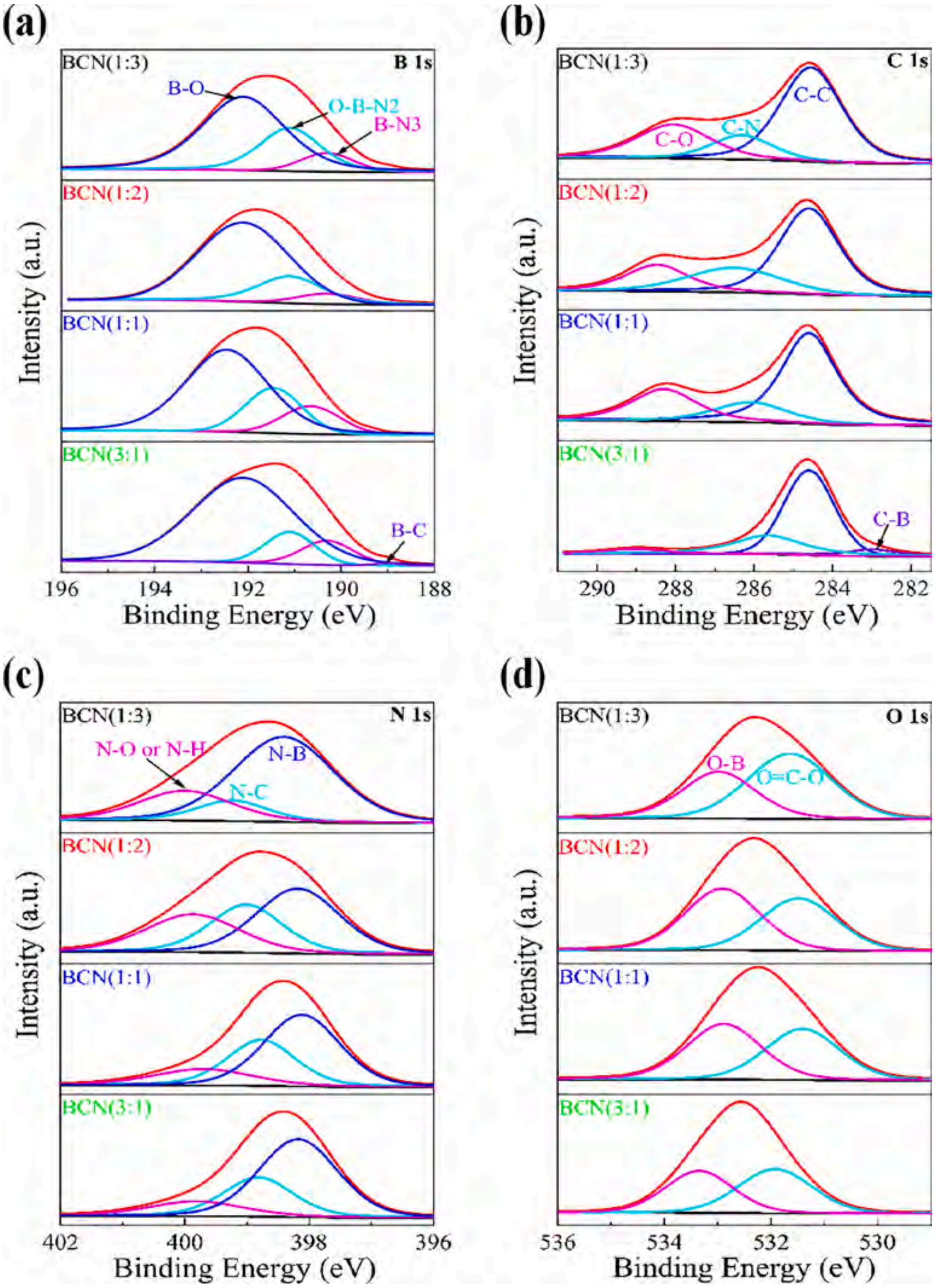

Fig. 3. XPS spectra of B 1s (a), C 1s (b), N 1s (c) and O 1s (d) of series BCN adsorbents.

B (283 eV), C–C (284.6 eV), C-N (286.3 eV) and C-O (288 eV), where the C-B bond is only observed in the adsorbent of BCN (3:1).[32,33] The main N 1s spectrum (Fig. 3c) signal peak originates from the N-B peak at 398.4 eV. In addition to this, there are two higher binding energy peaks located at 399.3 eV and 400 eV, respectively. And they may come from N-C and N-O or N–H bonding structures, respectively.[23,34] For the O element (Fig. 3d), the peak located at 531.6–531.9 eV is attributed to the O = C-O bond. While the peaks at 533.0–533.3 eV are attributed to the O-B bonding configurations.[1,35] The XPS binding peaks for the O = C-O bonds of BCN (3:1) are significantly lower compared to other higher carbon doped BCNs, suggesting that as the carbon content increases, the BCN material receives more electrons and therefore moves to a lower binding energy position.

The carbon in BCN is mainly derived from the raw material with the increase in the amount of melamine, the proportion of carbon in BCN gradually increases, while the content of boron gradually decreases. This trend of content change is not observed in the other two elements (N and O) (Table 1), which we speculate may be due to the partial replacement of B atoms by C atoms in melamine during the synthesis of BCN.

3.2. CO_2 capture capacity under UV irradiation

Due to the Lewis acidity of CO_2 molecules, it is possible to enhance the electron donating ability of the adsorbent through electron injection strategy, thereby enhancing its adsorption capacity for CO_2.[36] Carbon doping can regulate the band width of BN materials, and the generated BCN materials can be excited to generate photogenerated electrons under appropriate wavelength irradiation. Furthermore, improve its adsorption capacity for CO_2 molecules. We first tested the semiconductor properties of the synthesized BCN material through Hall effect tests (Table 3), confirming its electron donating ability.

Subsequently, in order to investigate the enhanced characteristics of CO_2 adsorption in BCN samples under light irradiation, we irradiated the BCN with 365 nm UV lamp during the adsorption process to generate more free electrons. Then we performed CO_2 adsorption isotherm tests on the synthesized BCN adsorbent at 298 K (without UV irradiation, Fig. 4a and with UV irradiation, Fig. 4b). To visualize more changes in CO_2 uptake, we plotted the adsorption capacity of BCN adsorbents before and after UV irradiation at 1 bar and 0.15 bar CO_2 (Fig. 4c and 4d). Interestingly, the results showed that all adsorbents presented remarkable increase in CO_2 adsorption capacity after UV irradiation. Among them, the BCN(1:3) adsorbent showed the greatest improvement after UV irradiation, and its CO_2 adsorption capacity improved from 1.29 (0.53) to 1.66 (0.70) mmol/g, which is increased by 28.7 %(1 bar) and 32.1 %(0.15 bar) compared to the dark tests, respectively. The other three BCN adsorbents also showed a significant increase in CO_2 adsorption capacity after UV irradiation. At a CO_2 partial pressure of 1 bar, the adsorption capacities of BCN (1:2), BCN (1:1) and BCN (3:1) rose from 1.23 to 1.38 mmol/g, 2.04 to 2.38 mmol/g, and 0.63 to 0.78 mmol/g, with the growth rate of adsorption capacity of 14.6 %, 16.7 % and 23.8 %, respectively. At a CO_2 partial pressure of 0.15 bar, the adsorption capacity of BCN (1:2), BCN (1:1), and BCN (3:1) were observed to had increased from 0.48 to 0.54 mmol/g, 0.73 to 0.91 mmol/g, and 0.19 to 0.25 mmol/g, with growth rates of adsorption capacity of 12.5 %, 24.6 %, and 31.5 %, respectively. The commercial hexagonal boron nitride (h-BN) material, as a counterpart, has a low CO_2 adsorption capacity of 0.013 mmol/g due to its weak van der Waals force bonding with CO_2. The BCN (1:3) synthesized in this work has 99 times higher adsorption capacity under CO_2 partial pressure of 1 bar and 25 °C, while it can have noticeable CO_2 adsorption capacity increasing under UV irradiation conditions. This is attributed to the doping of C and O elements into the BN lattice to form a large number of lattice defects, forming an n-type semiconductor material. As a result, the material exhibits excellent optoelectronic properties, while the BN material does not exhibit similar properties. Table 2 shows the comparison of the adsorption capacities of h-BN and BCN materials before and after UV irradiation at a CO_2 partial pressure of 1 bar and 25 °C.

3.3. Study the mechanism of UV light enhanced CO_2 adsorption

To explain the mechanism of enhanced CO_2 adsorption by BCN adsorbents under UV light irradiation, we had characterized the light absorption properties as well as the photoelectric properties of BCN adsorbents. The light absorption characteristics of the BCN adsorbents were examined by UV–Vis diffuse reflectance spectroscopy, as shown in Fig. 5a. The light absorption edge of the BCN adsorbent was gradually

Table 2
CO_2 adsorption capacity of h-BN and BCN adsorbents in the dark state and UV-illuminated state at 1 bar, 25 °C.

Adsorbents	CO_2 adsorption capacity - in dark state (mmol/g)	CO_2 adsorption capacity - UV irradiation state (mmol/g)
BCN(1:3)	1.29	1.66
BCN (1:2)	1.23	1.38
BCN (1:1)	2.04	2.38
BCN (3:1)	0.63	0.78
h-BN	0.013	0.013

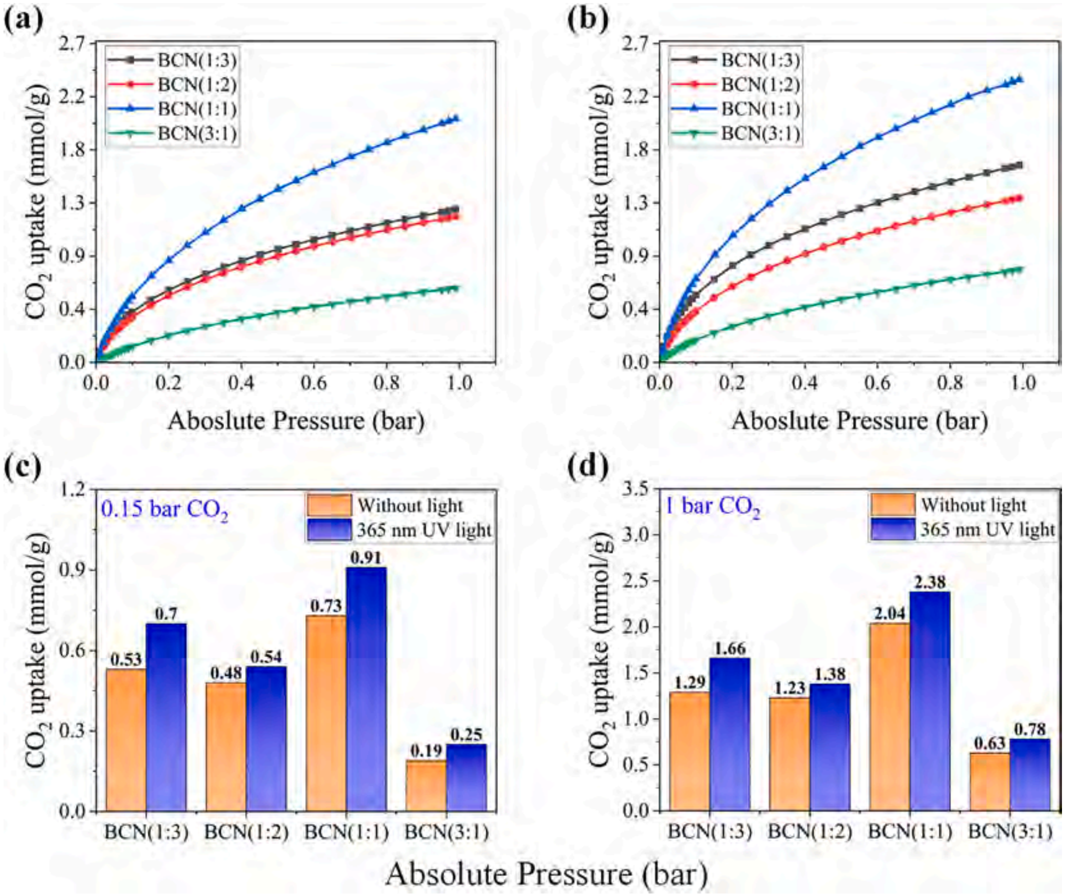

Fig. 4. CO_2 adsorption isotherms of BCN adsorbent at 298 K before (a) and after (b) UV irradiation. Comparison of CO_2 adsorption before and after UV irradiation at 365 nm under 298 K, 0.15 bar (c) and 1 bar (d) CO_2 partial pressure (Data derived from the CO_2 sorption isotherms in (a) and (b)).

Table 3
Hall effect test data of BCN(1:3) adsorbent before and after UV irradiation.

Adsorbent	Resistivity (ohm·cm)	Mobility ($cm^2/V{\cdot}S$)	Carrier concentration ($1/cm^3$)	Hall factor (cm^3/C)	f-factor
BCN(1:3) without UV irradiation	0.7755	0.01678	4.80×10^{20}	−0.01301	0.9872
BCN(1:3) after UV irradiation	0.7525	0.01675	5.42×10^{20}	−0.00944	0.9872

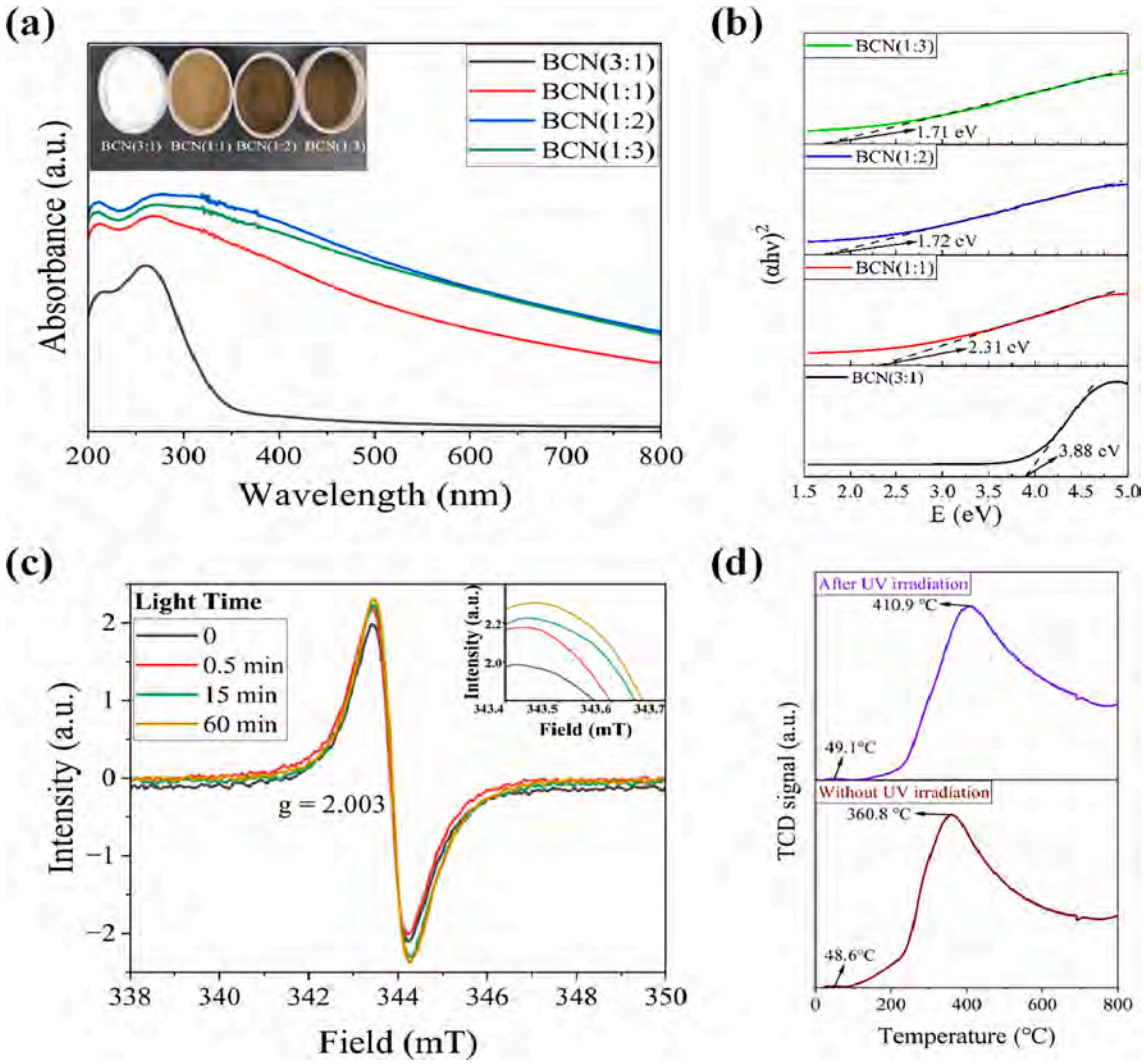

Fig. 5. (a) UV–Vis diffuse reflectance spectra of BCN adsorbents with optical image insets. (b) Bandgap calculation of BCN on UV–Vis diffuse reflectance spectra. The band gap is calculated based on the Tauc relation of $(\alpha h\upsilon)^2 = A(h\upsilon\text{-}E_g)$, where α, h, υ, A and E_g refer to the absorption coefficient, Planck's constant, optical frequency, constant and band gap of the semiconductor. (c) Room temperature in situ light EPR spectra of BCN(1:3), the illustration in the upper right corner is a partial enlargement. (d) CO_2-TPD curves of BCN(1:3) during CO_2 adsorption without and after 2 h of UV light irradiation.

red-shifted with increasing carbon content. The optical inset in the upper left corner of Fig. 5a shows the gradual light to dark color of the adsorbent, indicating that the visible band absorption of the BCN adsorbent also increases with rising carbon content. The h-BN without heteroatom doping is a typical insulator with a band gap of about 5.6 eV.[37,38] The band gaps of the synthesized adsorbents are smaller than this value due to the doping of C and O elements. Based on the Tauc plot in Fig. 5b, the band gap width of BCN(1:3) was estimated to be 1.71 eV, and the bandgap values of BCN(1:2), BCN(1:1), BCN(3:1) increase sequentially to 1.72 eV, 2.31 eV, and 3.88 eV, respectively. Long absorption tails in the visible light indicate the presence of in-band impurity jumps, possibly located at the surface.[39] All BCN adsorbents exhibit excellent light absorption properties in the UV wavelength range. The later photochemical characterization evidence can show that the optical properties of BCN are sufficient to change the electronic structure of the material by absorbing photons, generating more electrons to enhance the adsorption of CO_2 molecules.

To confirm whether light excites free electrons in the BCN adsorbents, we performed electron paramagnetic resonance (EPR) tests of BCN(1:3) with in situ irradiation. As shown in Fig. 5c, a strong electron paramagnetic resonance signal is detected for BCN(1:3) at a magnetic field strength of about 343.4 mT, and the calculated g-value is about 2.003, which is symmetric and suggests that the g-value corresponds to an isotropic homogeneous free electron species.[40,41] The EPR signal of the adsorbent was enhanced with increasing time of light exposure. When the adsorbent were continuously irradiated with mercury light for 0.5 and 60 min, the EPR peak intensity of porous BCN increased by approximately 10 % and 16 %, respectively. Thus, irradiation of the BCN adsorbents causes the accumulation of free electrons with time, and this process does not increase linearly, and the accumulation of free electrons becomes slower with time. The enhancement of the signal may be due to the release of captured charges under irradiation or the generation of electron-hole pairs.[39,42].

To further determine the effect of UV irradiation on the interaction between BCN and CO_2, we performed CO_2-TPD tests on BCN(1:3) before and after UV light irradiation. Generally, the basic centers are classified into three types based on the desorption temperature, including weakly basic centers (120–350 °C), moderately basic centers (350–600 °C), and strongly basic centers (>600 °C).[43,44] The CO_2-TPD plots of BCN(1:3) adsorbents before and after UV lamp irradiation are shown in Fig. 5d, where the desorption peak near 49 °C can be attributed to physical adsorption arising from the specific surface area.[45] The signal of the higher temperature desorption peaks shows a turning point at ~ 230 °C, and we attribute the signal of the desorption peaks from ~ 100–230 °C to the adsorption of –OH groups and $–NH_2$ groups, while the moderately basic centers at higher temperatures are generated by structural defects.[46–48] Specifically, under the initial conditions, the desorption peak of the BCN(1:3) adsorbent at 360.8 °C should be caused by a large number of defects generated by the carbon doping. Carbon doping can induce the necessary negative charge on BCN. Thus, BCN with the necessary negative charge can induce charge-induced chemisorption, which enhances the binding of CO_2 to the BCN(1:3) surface.[49,50] The desorption peak of the BCN(1:3) adsorbent shifted toward higher temperatures (from 360.8 to 410.9 °C) after UV irradiation. These results suggest that UV irradiation enhances the binding strength of CO_2 to BCN (1:3), specifically UV irradiation excites more negative charges in the material, which makes the interaction stronger. Then we tested the transient photocurrent response of a series of BCN adsorbents under UV light to study the light responsiveness of these adsorbents (Fig. 6). Only BCN (3:1) showed poor photocurrent response, while all other adsorbents showed good photocurrent response, indicating that carbon doping facilitated the transfer of these photoexcited electrons to the BCN surface.

Hall effect tests can further provide us with more quantitative insight into the electron changes in BCN adsorbents before and after UV irradiation (Table 3). Since the Hall factor is negative in the test results (Table 3), it indicates that the electrons in the BCN(1:3) sample are majority carriers, thus it can be determined that BCN(1:3) is an N-type semiconductor material. The resistivity of BCN(1:3) decreased significantly after UV irradiation, and the carrier concentration increased from $4.80 \times 10^{20}/cm^3$ to $5.42 \times 10^{20}/cm^3$, increasing the carrier concentration by about 12.9 %. This is sufficient to prove that UV irradiation of BCN material can make the material produce more free electrons, enhancing the electron-donating ability of the material and strengthen its interaction with CO_2. The slight decrease in mobility after UV irradiation is due to the increased scattering between carriers, which hinders their free movement in the material. This scattering includes the interaction between electrons and holes, as well as the interaction of carriers with defects.

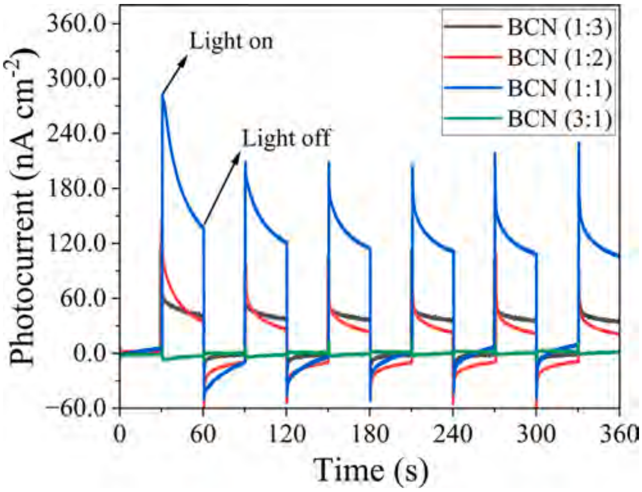

Fig. 6. Photocurrent versus time (I–t) curves of BCN adsorbents.

Based on our above characterization it can be demonstrated that the BCN (1:3) adsorbent can be excited with more free electrons under UV irradiation. In order to further verify whether the increase of free electrons enhances the adsorption of CO_2 on the BCN adsorbent, we carried out a density functional theory (DFT) computation for this adsorption system before and after the injection of additional electrons. This BCN model is based on previous researchers' DFT studies on the crystal structure of C and O co-doped boron nitride, and the model and related calculations had been successfully used to characterize such materials.[27,51,52].

The elemental ratios of the model were matched based on the elemental ratios of the actual BCN (1:3) adsorbent, where the atomic numbers B:C:N:O = 16:10:15:19. We performed adsorption energy calculations for BCN (1:3) adsorbent with CO_2 before and after injection of electrons (with an additional injection of 1 e^-) (Fig. 7). The O-B-N2 site and B-N3 site were selected as adsorption sites, respectively. And the changes of CO_2 adsorption energy at these two sites were observed before and after electron injection. It can be found that the adsorption energies of different adsorption sites were greatly improved after the additional injection of 1 e^-, in which the O-B-N2 site was increased from the initial −4.80 eV to −8.93 eV, which can confirm that the additional free electrons can strengthen the adsorption strength of BCN adsorbents with CO_2, and thus improve the adsorption capacity of BCN adsorbent.

Based on the above analysis and findings, a rational mechanism for the enhancement of CO_2 capture capacity by light-induced BCN adsorbent was proposed. The mechanism of photo-induced generation of free electrons to enhance the CO_2 capture capacity is shown in Fig. 8. The BCN adsorbents synthesized in this study is an N-type semiconductor material, which can generate a large number of free electrons under light irradiation. At the same time, the B atom in the BCN material serves as the electron obtaining center, and the generated free electrons will gather around the B atom. As a Lewis acidic molecule, the higher concentration of electrons in the local domain is conducive for the BCN adsorbent to produce a stronger binding force on the CO_2 molecule. Meanwhile, in consideration of the lower thermal effect of UV light can avoid the CO_2 desorption caused by the photothermal effect, we used UV light for the first time to irradiate the BCN adsorbents when it adsorbs CO_2, and the CO_2 adsorption capacity of BCN samples can be significantly improved after UV irradiation.

4. Conclusion

In summary, we proposed and demonstrated a new strategy to enhance the CO_2 adsorption performance of solid adsorbent by light irradiation. N-type semiconductor BCN materials were synthesized by a simple high-temperature pyrolysis method and used as CO_2 photo-responsive adsorbents. The band gap of the synthesized BCN materials can be adjusted by changing the ratio of boric acid/melamine in the raw materials, and the abundant structural defects endowed the BCN materials with excellent CO_2 adsorption capacity. The binding force of the BCN adsorbents with CO_2 molecules was enhanced by UV irradiation to stimulate more free electrons, thus improving its adsorption capacity. The experimental results showed that the highest increase in the CO_2 adsorption capacity of the BCN (1:3) adsorbent was achieved after UV irradiation, with the CO_2 adsorption capacity increasing from 1.29 mmol/g to 1.66 mmol/g at 1 bar, 298 K, which is an enhancement of ~ 32 %. Solar energy is an important renewable source, and exploring the use of sunlight to drive CO_2 capture system will greatly reduce the cost and protect the environment. In this study, we experimentally verified the enhanced CO_2 capture ability driven by light energy and achieved the regulation of CO_2 adsorption capacity. This provides a new approach for industrial level applications of low-cost CO_2 capture and utilization.

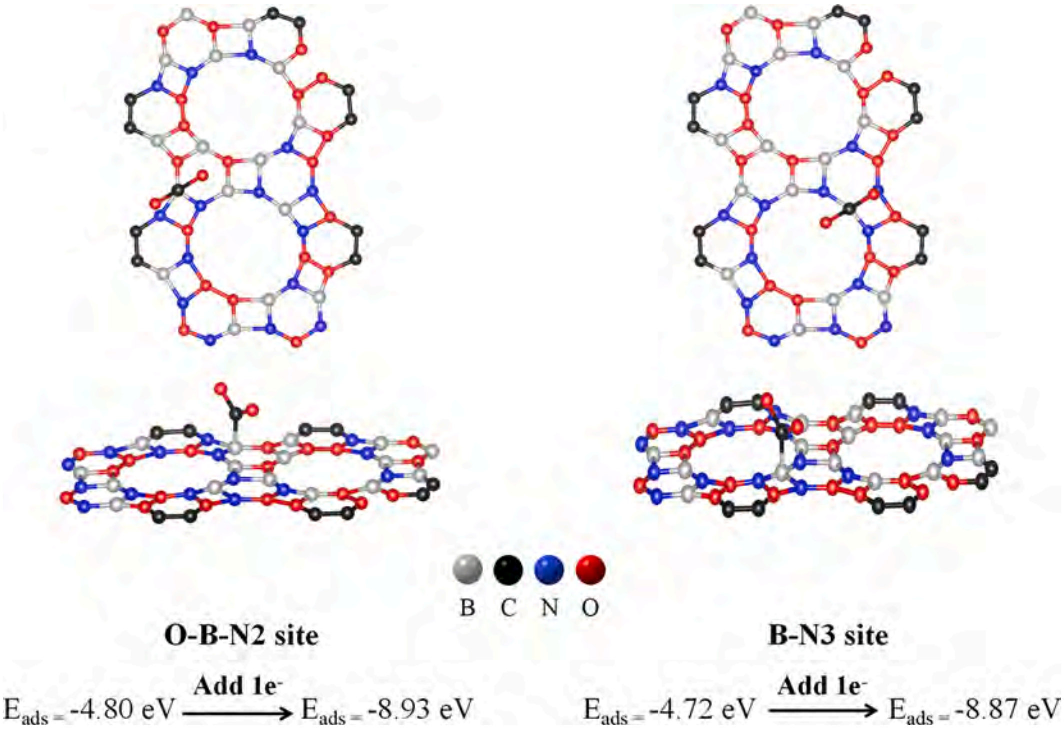

Fig. 7. CO_2 adsorption energies of the optimized structures of BCN (1:3) adsorbent with O-B-N2 sites and B-N3 sites in the initial state and after additional injection of $1e^-$.

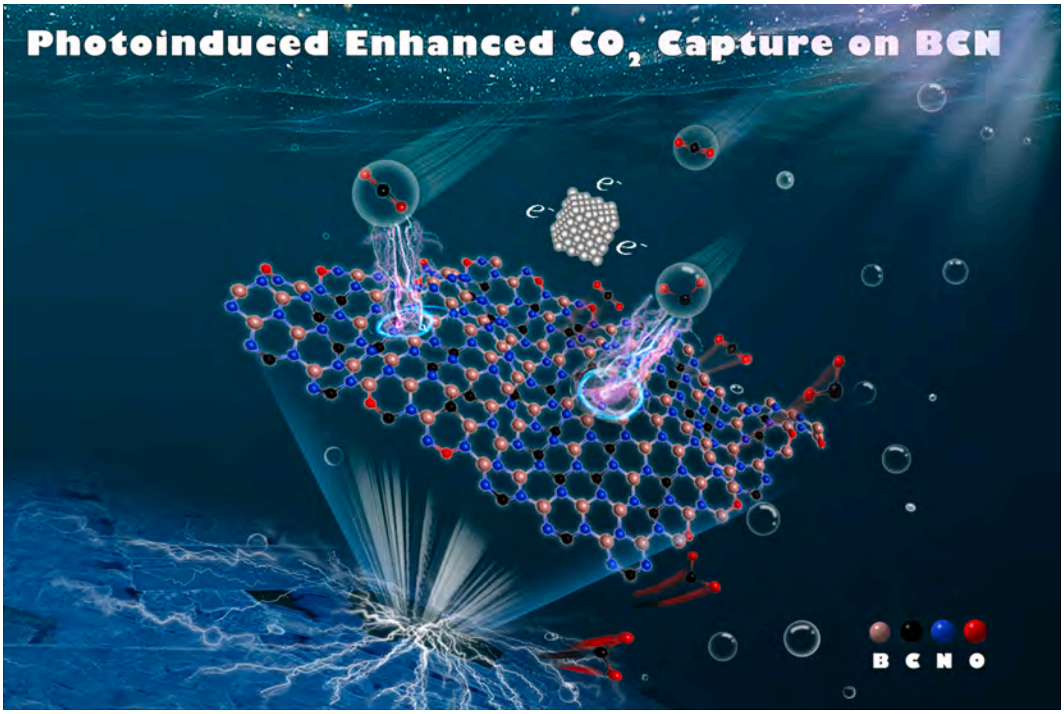

Fig. 8. Schematic diagram of photo-induced electron generation for enhanced CO_2 capture capacity.

CRediT authorship contribution statement

Xiaoyu Duan: Writing – original draft, Methodology, Investigation, Data curation. **Guanqing Song:** Validation, Software, Investigation, Formal analysis. **Chi Song:** Validation, Resources, Methodology. **Guanhong Lu:** Validation, Software, Investigation, Formal analysis. **Yan Wang:** Visualization, Software, Resources. **Jing Sun:** Supervision, Project administration, Conceptualization. **Aiying Chen:** Writing – review & editing, Supervision, Funding acquisition, Conceptualization. **Xiaofeng Xie:** Writing – review & editing, Supervision, Funding acquisition, Conceptualization.

Declaration of competing interest

The authors declare that they have no known competing financial interests or personal relationships that could have appeared to influence the work reported in this paper.

Data availability

Data will be made available on request.

Acknowledgments

This work was financially supported by the National Key Research and Development Program of China (2021YFE0110400); the National Natural Science Foundation of China (52072387); Inner Mongolia Key R&D Plan (2022YFHH0049).

Appendix A. Supplementary data

Supplementary data to this article can be found online at https://doi.org/10.1016/j.seppur.2024.126685.

References

[1] Y. Li, L. Liu, H. Yu, et al., Synergy of developed micropores and electronic structure defects in carbon-doped boron nitride for CO2 capture, Sci. Total Environ. 811 (2022).
[2] P.D. Dissanayake, S.W. Choi, A.D. Igalavithana, et al., Sustainable gasification biochar as a high efficiency adsorbent for CO2 capture: A facile method to designer biochar fabrication, Renew. Sustain. Energy Rev. 124 (2020).
[3] D.P. Hanak, E.J. Anthony, V. Manovic, A review of developments in pilot-plant testing and modelling of calcium looping process for CO2 capture from power generation systems, Energ. Environ. Sci. 8 (8) (2015) 2199–2249.
[4] J. Kou, L.B. Sun, Fabrication of nitrogen-doped porous carbons for highly efficient CO2 capture: rational choice of a polymer precursor, J. Mater. Chem. A 4 (44) (2016) 17299–17307.
[5] D. Golberg, Y. Bando, C.C. Tang, et al., in: Boron Nitride Nanotubes and Nanosheets - Introduction and Recent Advances, Wiley-VCH Verlag, 2007, pp. 2413–2432.
[6] M. Corso, W. Auwarter, M. Muntwiler, et al., Boron nitride nanomesh, Science 303 (5655) (2004) 217–220.
[7] M. Yi, Z. Shen, X. Zhao, et al., Boron nitride nanosheets as oxygen-atom corrosion protective coatings, Appl. Phys. Lett. 104 (14) (2014).
[8] A. Du, Y. Chen, Z. Zhu, et al., Dots versus Antidots: Computational Exploration of Structure, Magnetism, and Half-Metallicity in Boron-Nitride Nanostructures, J. Am. Chem. Soc. 131 (47) (2009) 17354–17359.
[9] A. Du, Y. Chen, Z. Zhu, et al., C-BN Single-Walled Nanotubes from Hybrid Connection of BN/C Nanoribbons: Prediction by ab initio Density Functional Calculations, J. Am. Chem. Soc. 131 (5) (2009) 1682–1683.
[10] M.P. Levendorf, C.-J. Kim, L. Brown, et al., Graphene and boron nitride lateral heterostructures for atomically thin circuitry, Nature 488 (7413) (2012) 627–632.
[11] C. Yang, D. Liu, Y. Chen, et al., Three-Dimensional Functionalized Boron Nitride Nanosheets/ZnO Superstructures for CO2 Capture, ACS Appl. Mater. Interfaces 11 (10) (2019) 10276–10282.
[12] S. Marchesini, C.M. McGilvery, J. Bailey, et al., Template-Free Synthesis of Highly Porous Boron Nitride: Insights into Pore Network Design and Impact on Gas Sorption, ACS Nano 11 (10) (2017) 10003–10011.
[13] R. Mighri, U.B. Demirci, J.G. Alauzun, Microporous Borocarbonitrides BxCyNz: Synthesis, Characterization, and Promises for CO2 Capture, Nanomaterials 13 (4) (2023).
[14] H. Guo, W. Zhang, N. Lu, et al., CO2 Capture on h-BN Sheet with High Selectivity Controlled by External Electric Field, J. Phys. Chem. C 119 (12) (2015) 6912–6917.
[15] X. Li, B. Lin, H. Li, et al., Carbon doped hexagonal BN as a highly efficient metal-free base catalyst for Knoevenagel condensation reaction, Appl. Cataly. B-Environ. 239 (2018) 254–259.
[16] J. Pang, Y. Chao, H. Chang, et al., Tuning electronic properties of boron nitride nanoplate via doping carbon for enhanced adsorptive performance, J. Colloid Interface Sci. 508 (2017) 121–128.
[17] A. Conde-Gonzalez, M. Glinka, D. Dutta, et al., Rapid fabrication and screening of tailored functional 3D biomaterials: Validation in bone tissue repair-Part II, Biomater. Adv. (2023) 145.
[18] L. Ci, L. Song, C. Jin, et al., Atomic layers of hybridized boron nitride and graphene domains, Nat. Mater. 9 (5) (2010) 430–435.
[19] J. Lu, K. Zhang, X.F. Liu, et al., Order-disorder transition in a two-dimensional boron-carbon-nitride alloy, Nat. Commun. (2013) 4.
[20] C. Gautam, C.S. Tiwary, S. Jose, et al., Synthesis of Low-Density, Carbon-Doped, Porous Hexagonal Boron Nitride Solids, ACS Nano 9 (12) (2015) 12088–12095.
[21] Y. Yang, Z. Shen, H. Yang, et al., Construction adsorption and photocatalytic interfaces between C, O co-doped BN and Pd-Cu alloy nanocrystals for effective conversion of CO2 to CO, J. Colloid Interface Sci. 640 (2023) 949–960.
[22] S. Chen, P. Li, S. Xu, et al., Carbon doping of hexagonal boron nitride porous materials toward CO2 capture, J. Mater. Chem. A 6 (4) (2018) 1832–1839.
[23] C. Huang, C. Chen, M. Zhang, et al., Carbon-doped BN nanosheets for metal-free photoredox catalysis . Nature, Communications (2015) 6.
[24] J. Wu, L. Wang, B. Lv, et al., Facile Fabrication of BCN Nanosheet-Encapsulated Nano-Iron as Highly Stable Fischer-Tropsch Synthesis Catalyst, ACS Appl. Mater. Interfaces 9 (16) (2017) 14319–14327.
[25] T. Yuan, Z. Wu, S. Zhai, et al., Photosynthetic Fixation of CO2 in Alkenes by Heterogeneous Photoredox Catalysis with Visible Light, Angew. Chem.-Int. Ed. (2023).
[26] R. Goyal, B. Sarkar, A. Bag, et al., Single-step synthesis of hierarchical BxCN: a metal-free catalyst for low-temperature oxidative dehydrogenation of propane, J. Mater. Chem. A 4 (47) (2016) 18559–18569.
[27] J. Liang, Q. Song, J. Lin, et al., In Situ Cu-Loaded Porous Boron Nitride Nanofiber as an Efficient Adsorbent for CO2 Capture, ACS Sustain. Chem. Eng. 8 (19) (2020) 7454–7462.
[28] J. Wang, J. Hao, D. Liu, et al., Flower stamen-like porous boron carbon nitride nanoscrolls for water cleaning, Nanoscale 9 (28) (2017) 9787–9791.
[29] Z. Shen, Y. Song, C. Yin, et al., Construction of hierarchically porous 3D graphene-like carbon material by B, N co-doping for enhanced CO2 capture, Micropor. Mesopor. Mater. 322 (2021) 111158.
[30] T. Shen, S. Liu, W. Yan, et al., Highly efficient preparation of hexagonal boron nitride by direct microwave heating for dye removal, J. Mater. Sci. 54 (12) (2019) 8852–8859.
[31] L. Li, C. Hu, L. Zhang, et al., Framework Cu-doped boron nitride nanobelts with enhanced internal electric field for effective Fenton-like removal of organic pollutants, J. Mater. Chem. A 7 (12) (2019) 6946–6956.
[32] H. Huang, S. Li, B. Chen, et al., Endoplasmic reticulum-targeted polymer dots encapsulated with ultrasonic synthesized near-infrared carbon nanodots and their application for in vivo monitoring of Cu2+, J. Colloid Interface Sci. 627 (2022) 705–715.
[33] Y. Cao, Z. Geng, W. Chen, et al., Introduction of carbon-boron atomic groups as an efficient strategy to boost formic acid production toward CO2 electrochemical reduction, Chem. Commun. 54 (27) (2018) 3367–3370.
[34] Y. Xue, P. Dai, X. Jiang, et al., Template-free synthesis of boron nitride foam-like porous monoliths and their high-end applications in water purification, J. Mater. Chem. A 4 (4) (2016) 1469–1478.
[35] J.I. Mendez-Linan, E. Ortiz-Ortega, M.F. Jimenez-Moreno, et al., Aging effect of plasma-treated carbon surfaces: An overlooked phenomenon, Carbon 169 (2020) 32–44.
[36] Q. Sun, Z. Li, D.J. Searles, et al., Charge-Controlled Switchable CO2 Capture on Boron Nitride Nanomaterials, J. Am. Chem. Soc. 135 (22) (2013) 8246–8253.
[37] K. Watanabe, T. Taniguchi, H. Kanda, Direct-bandgap properties and evidence for ultraviolet lasing of hexagonal boron nitride single crystal, Nat. Mater. 3 (6) (2004) 404–409.
[38] L. Song, L. Ci, H. Lu, et al., Large Scale Growth and Characterization of Atomic Hexagonal Boron Nitride Layers, Nano Lett. 10 (8) (2010) 3209–3215.
[39] C. Huang, C. Chen, M. Zhang, et al., Carbon-doped BN nanosheets for metal-free photoredox catalysis, Nat. Commun. 6 (1) (2015) 7698.
[40] Q. Weng, D.G. Kvashnin, X. Wang, et al., Tuning of the Optical, Electronic, and Magnetic Properties of Boron Nitride Nanosheets with Oxygen Doping and Functionalization, Adv. Mater. 29 (28) (2017).
[41] W. Lin, H. Chen, G. Lin, et al., Creating Frustrated Lewis Pairs in Defective Boron Carbon Nitride for Electrocatalytic Nitrogen Reduction to Ammonia, Angew. Chem.-Int. Ed. 61 (36) (2022).
[42] R. Shankar, M. Sachs, L. Francas, et al., Porous boron nitride for combined CO2 capture and photoreduction, J. Mater. Chem. A 7 (41) (2019) 23931–23940.
[43] B. Ali, S. Yusup, A.T. Quitain, et al., Synthesis of novel graphene oxide/bentonite bi-functional heterogeneous catalyst for one-pot esterification and transesterification reactions, Energ. Conver. Manage. 171 (2018) 1801–1812.
[44] X. Song, D. Pan, Y. Wu, et al., Synthesis of glycerol carbonate over porous La-Zr based catalysts: The role of strong and super basic sites, J. Alloy. Compd. 750 (2018) 828–837.
[45] K. Bu, J. Deng, X. Zhang, et al., Promotional effects of B-terminated defective edges of Ni/boron nitride catalysts for coking- and sintering-resistant dry reforming of methane, Appl Catal B 267 (2020) 118692.
[46] L. Wang, C. Wang, Z. Zhang, et al., Thermal induced BCN nanosheets evolution and its usage as metal-free catalyst in ethylbenzene dehydrogenation, Appl. Surf. Sci. 422 (2017) 574–581.
[47] C. Italiano, J. Llorca, L. Pino, et al., CO and CO2 methanation over Ni catalysts supported on CeO2, Al2O3 and Y2O3 oxides, Appl Catal B 264 (2020) 118494.
[48] M. Saghian, S. Dehghanpour, M. Sharbatdaran, Amine-functionalized frameworks as highly actives catalysts for chemical fixation of CO2 under solvent and co-catalyst free conditions, J. CO2 Util. 41 (2020) 101253.
[49] H. Choi, Y.C. Park, Y.-H. Kim, et al., Ambient Carbon Dioxide Capture by Boron-Rich Boron Nitride Nanotube, J. Am. Chem. Soc. 133 (7) (2011) 2084–2087.

[50] X. Tan, H.A. Tahini, S.C. Smith, Borophene as a Promising Material for Charge-Modulated Switchable CO2 Capture, ACS Appl. Mater. Interfaces 9 (23) (2017) 19825–19830.

[51] Y. Liu, L. Li, Q. Li, et al., Electronic properties and surface reactive sites of carbon and oxygen doped porous boron nitride: A DFT study, Diam. Relat. Mater. 121 (2022).

[52] Q. Li, L. Li, X. Yu, et al., Ultrafine platinum particles anchored on porous boron nitride enabling excellent stability and activity for oxygen reduction reaction, Chem. Eng. J. 399 (2020) 125827.